Supplementary Information

Toward Understanding CO Oxidation on High-Entropy Alloy Electrocatalysts

María Paula Salinas-Quezada,[1] Jack Pedersen,[1] Paula Sebastián-Pascual,[1] Ib Chorkendorff,[2] Krishanu Biswas,[3] Jan Rossmeisl,[*,1] María Escudero-Escribano[*,1,4,5]

[1] Department of Chemistry, Center for High Entropy Alloy Catalysis, University of Copenhagen, 2100 Copenhagen, Denmark

[2] Department of Physics, Surface Physics and Catalysis, Technical University of Denmark, 2800 Lyngby, Denmark

[3] Department of Materials Science and Engineering, Indian Institute of Technology Kanpur, 208016 Kanpur, India

[4] Catalan Institute of Nanoscience and Nanotechnology (ICN2), CSIC and Barcelona Institute of Science and Technology, UAB Campus, 08193 Bellaterra, Barcelona, Spain

[5] Catalan Institution for Research and Advanced Studies (ICREA), Pg. Lluís Companys 23, 08010 Barcelona, Spain

[*] Corresponding authors:

María Escudero-Escribano: maria.escudero@icn2.cat

Jan Rossmeisl: jan.rossmeisl@chem.ku.dk

To conduct CO stripping measurements, the surface electrodes were held at 0.2 V vs RHE. To ensure complete coverage of CO on the surface, the solution was saturated with CO for 10 minutes. Subsequently, the solution was bubbled with Ar to remove any excess of CO from the cell. Figure S1 shows the CO stripping curve of Pt, Pd, quaternary AuCuPdPt and AgAuCuPdPt High Entropy Alloy (HEA) in acidic media at a scan rate of 20 mVs^{-1}. Although it is most likely that CO only covers Pd and Pt sites in the HEA, we believe that the broadening of the CO stripping peaks on the HEA in comparison with Pd and Pt is due to the lack of *OH sites. This means that a higher overpotential is necessary to remove the CO adsorbed on the surface. The quaternary alloy behaves similarly to the HEA in this regard.
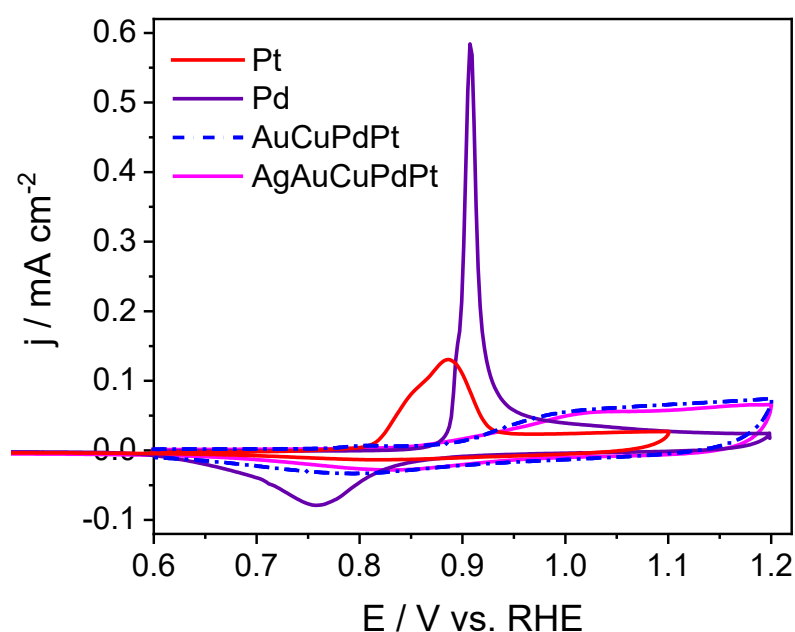

Figure S1. CO stripping curves of Pt poly (red line), Pd poly (purple line), extended quaternary AuCuPdPt (dotted blue line), and HEA (magenta line) in contact with 0.1 M HClO$_4$ saturated in Ar atmosphere at 20 mVs^{-1}.

Figure S2A displays five continuous voltammograms for CO oxidation on the HEA surface. The cyclic voltammograms do not show any significant changes except for a minor decrease in current density near 1.1 V vs RHE. It is worth noting that the onset potential for CO oxidation, which is highly dependent on composition, remains unchanged after five cycles. These results suggest that surface structure or composition changes upon consecutive cycles up to 1.1 V are very slow. On the other hand, Figure S2B showcases the blank cyclic voltammograms taken before and after CO oxidation on the HEA surface. This figure highlights that the charge in the hydrogen region increased after the oxidation of CO. Additionally, the onset of the oxide region is observed to be near 0.7 V vs RHE, which is lower than the potential measured before CO oxidation. By comparing these two blank voltammograms, we can gain insights into the changes or redistribution that have occurred on the surface of the HEA.
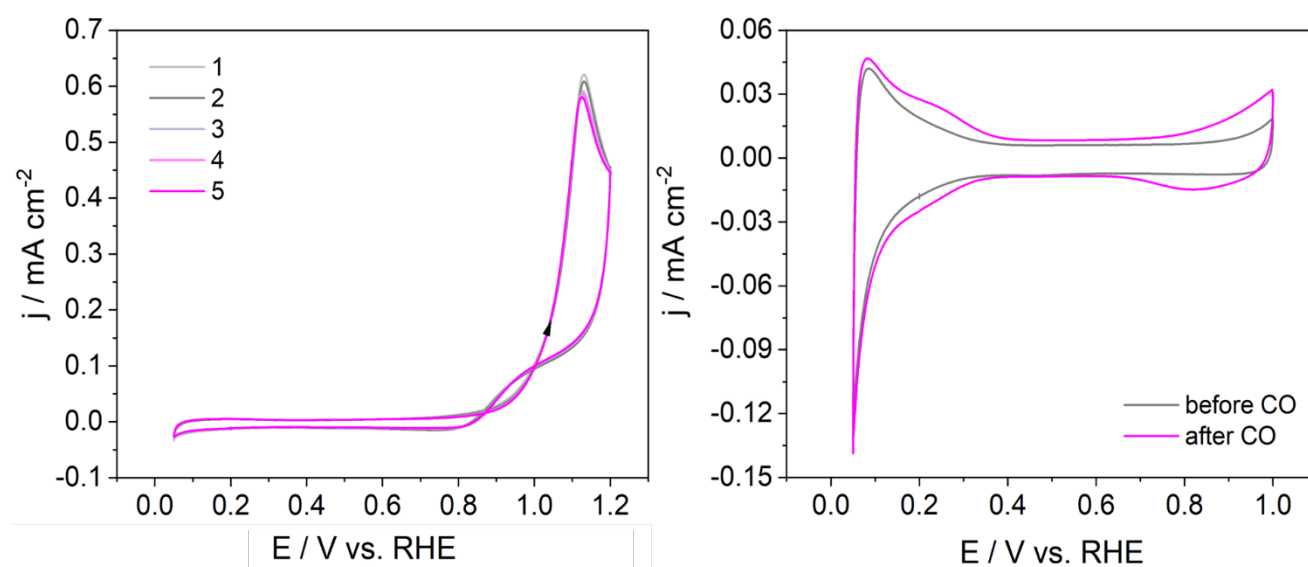

Figure S2.A) Five continuous CO oxidation curves of an extended AgAuCuPdPt HEA in a CO-saturated atmosphere. B) Blank voltammograms of the HEA before and after CO oxidation saturated in Ar atmosphere. All the experiments were performed at 50 mVs^{-1} in 0.1 M HClO$_4$.

Figure S3 shows the blank cyclic voltammograms of the HEA before and after the surface pre-treatment. The pre-treatment included cycling from -0.05 V to 1 V vs RHE at a scan rate of 500 mVs^{-1}. This range of potential was selected to remove any impurities that might have been absorbed on the surface. Higher potential values were avoided on the multimetallic electrodes to prevent any additional alteration or modification of the surface composition.
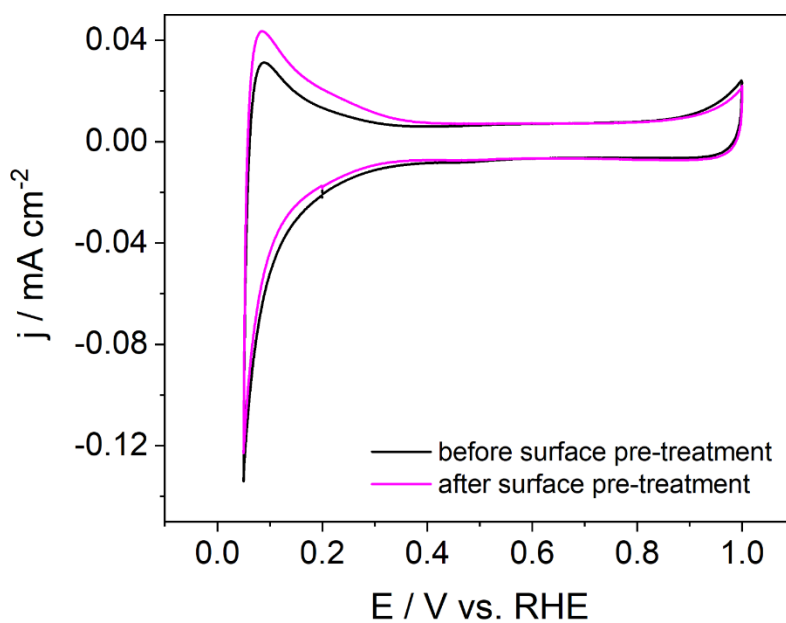

Figure S3. Blank cyclic voltammograms of the extended AgAuCuPdPt HEA, before and after the surface pre-treatment at 50 mVs^{-1} in 0.1 M HClO$_4$.

The position of the adventitious carbon (C 1s) was measured in the HEA, showing a variation of 0.5 eV before and after CO oxidation. We infer that this shift occurred due to the experiments being conducted on different days, which could have affected the measurement.
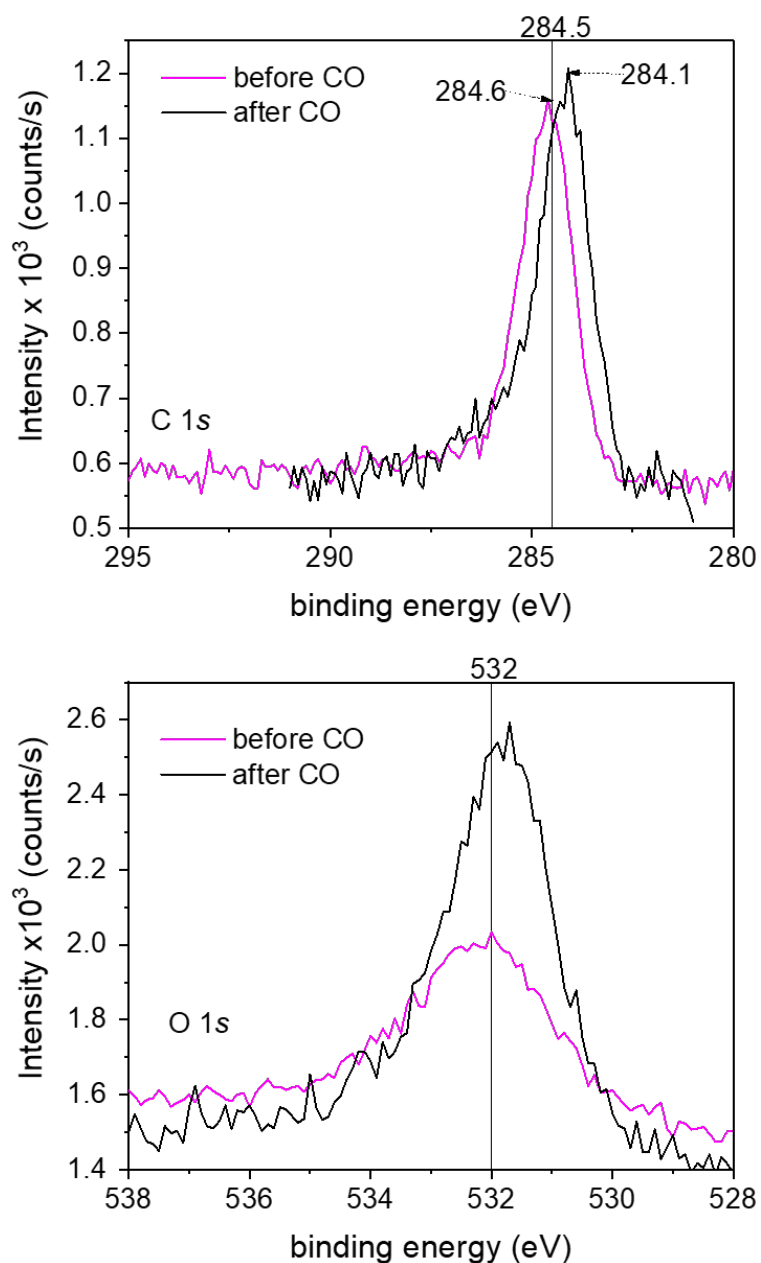

Figure S4. XPS spectra of C 1s and O 1s before and after CO oxidation, magenta and black lines, respectively.[1][2] The XPS spectra were collected with a pass energy of 50 eV with a step size of 0.1 eV and a dwell time of 50 ms for 50 scans.

Figure S5 displays the HEA survey spectra before and after CO oxidation. The survey spectra before CO oxidation were collected by setting the pass energy to 200 eV with a step size of 1 eV and a dwell time of 50 ms for 20 scans. However, the survey spectra after CO oxidation were collected with a pass energy of 50 eV with a step size of 1 eV and a dwell time of 50 ms for 5 scans. We believe that the main reason for the noise and not well-defined peaks in the survey spectra after CO oxidation is due to the samples were taken on different days and conditions.
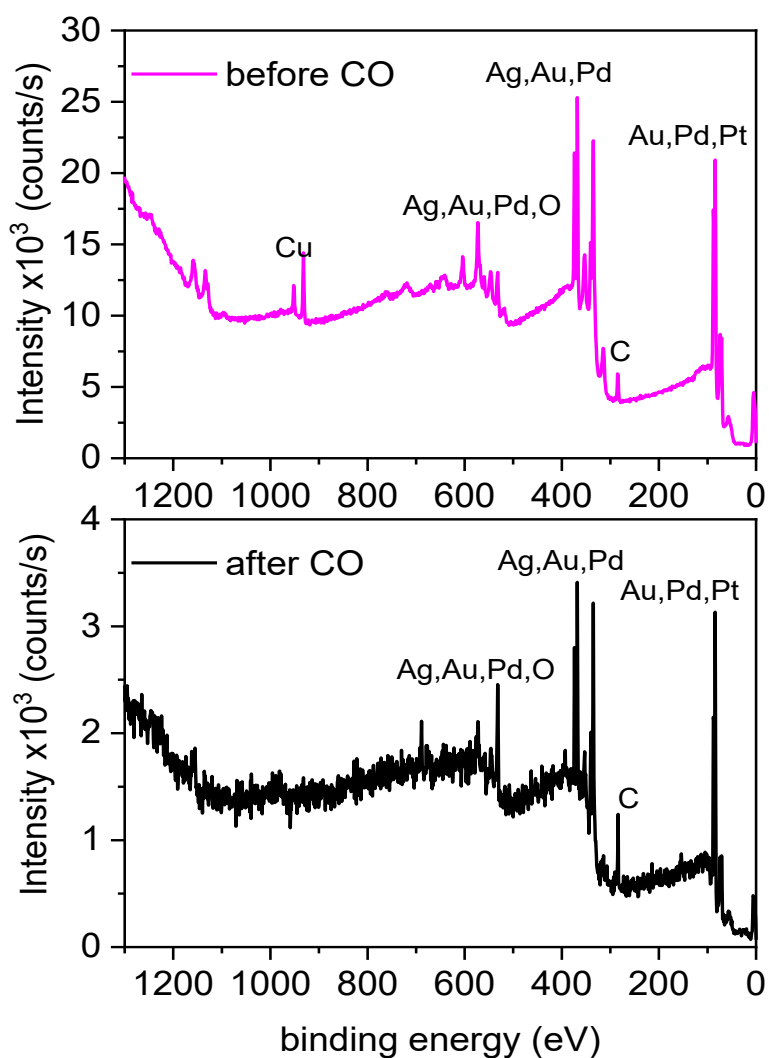

Figure S5. Survey scan of the HEA, before and after CO oxidation. [1] [2]

Figure S6 shows the angle-resolved XPS spectra for Cu *2p*, which were measured after CO oxidation at four different angles. This measurement technique allows deeper layers of the material to be probed by increasing the measurement angle. The spectra revealed that the amount of Cu in the deeper layers of the material did not increase, which indicates that Cu is not being reorganized back to the bulk. The measurements were taken at open circuit potential.
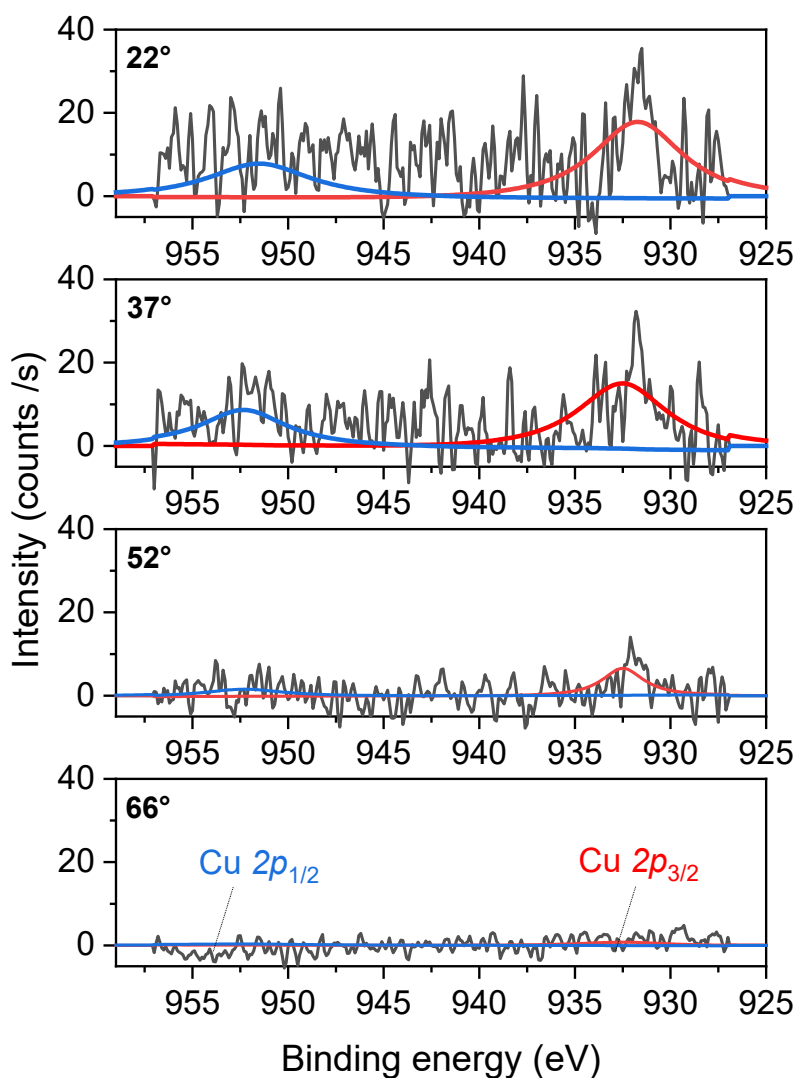

Figure S6. Angle-resolved XPS spectra of Cu *2p* are shown at four different measurement angles: 22°, 37°, 52°, and 66° after CO oxidation. The XPS spectra were collected with a pass energy of 50 eV, a step size of 0.1 eV, and a dwell time of 50 ms for 40 scans.

Table S1. Atomic percentages of each element in the extended bimetallic AuPd and quaternary AuCuPdPt alloys after continuous CO oxidation. The results were calculated from XPS measurements after 10 cycles in CO oxidation.

Element	Bimetallic Alloy AuPd	Quaternary Alloy AuCuPdPt
Pd	35 ± 3	38± 4
Au	67 ± 3	42± 4
Pt	-	19± 1
Cu	-	3± 1

$$\underline{x}_{CO} = [0,1, \quad 1,0,2,3, \quad 2,1,0,0, \quad 0,0,3,0, \quad 0,0,0,0,0,1,0, \quad 1, \quad 1 \quad]^T$$
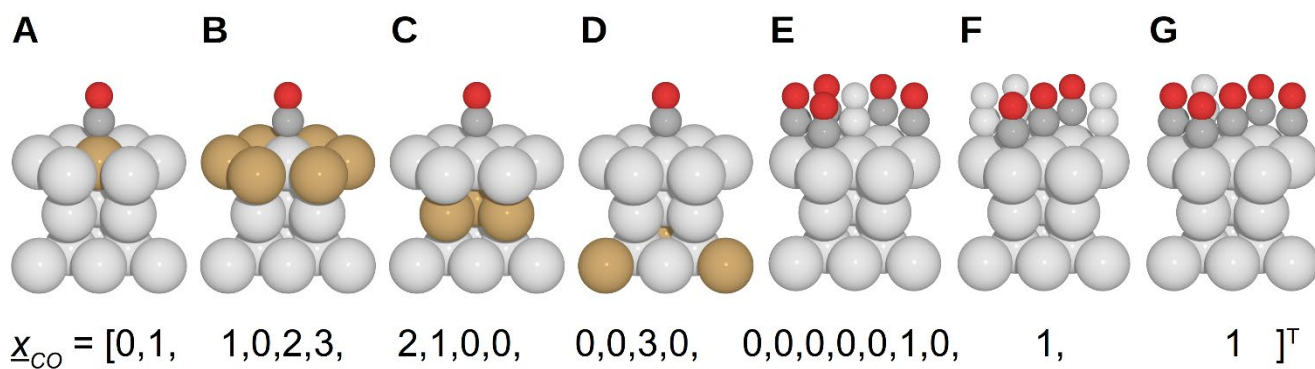
Figure S7. Feature construction for *CO adsorption energy predictions. **A-G**) The feature vector consists of 23 numbers: 2 for identifying the on-top adsorption site (Pd or Pt) (A); 4 obtained by counting the number of each element (in the order Ag, Au, Pd, and Pt) in the neighboring surface environment around the adsorbate (B); 4 by counting the elements in the neighboring subsurface (C); 4 by counting the elements in the next nearest zone of element in the 3rd layer (D); 7 for characterizing the number of *CO neighbors, a one-hot encoding of a number between 0 and 6 (E); 1 for identifying whether 3 adsorbates form a straight line (F); and 1 for identifying whether 5 adsorbates form an 'X' cross-shape (G). An example of a feature vector is given.
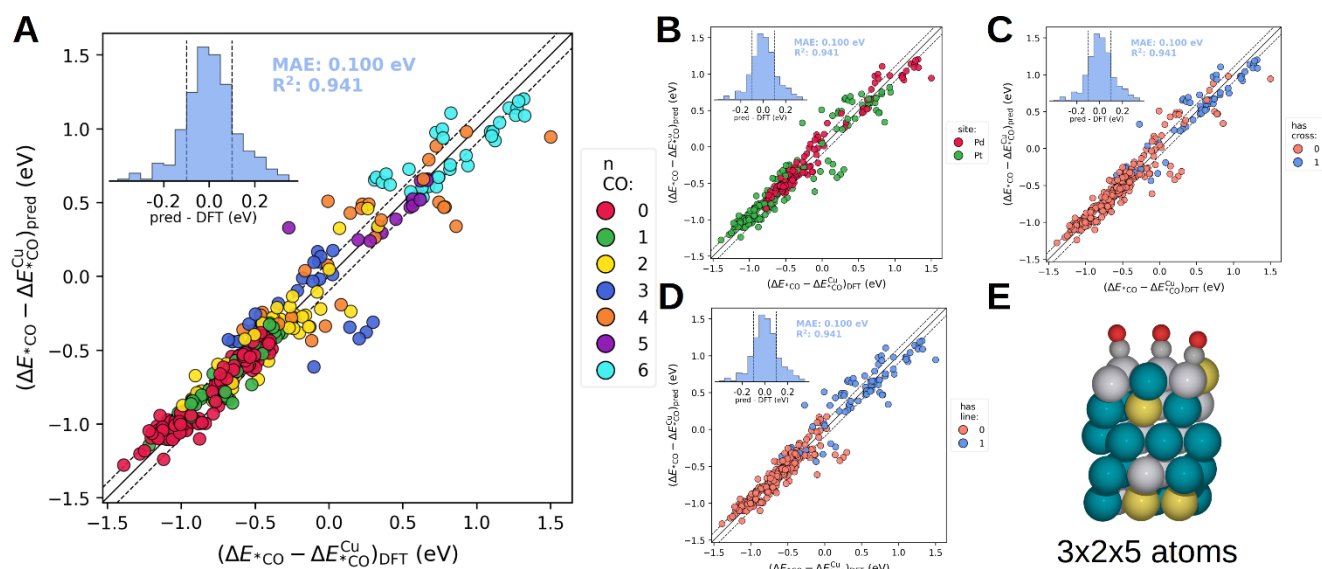
Figure S8. Performance of *CO adsorption energy predictions on a 3x2x5 atom training set. **A-D**) Parity plots showing the performance (mean absolute error: 0.100 eV, coefficient of determination, R^2: 0.941) of leave-one-out cross validations on linear regressors using 344 *CO adsorption energies obtained on periodic 3x2x5 atom surfaces. The parity plots have been colored according to number of *CO neighbors (A), adsorption site (B), whether an 'X' is formed by the adsorbates (C), and whether a straight line is formed by the adsorbates (D). **E**) Example of a periodically repeated 3x2x5 atom structure used for generating the input energies.

Table S2. Linear parameters used for predicting *CO adsorption energies relative to *CO on Cu(111). The parameters correspond to the feature vector illustrated in Figure S7. The set of features contain 5 redundant variables due to the fixed number of atoms in the zones around the adsorbate. This allows the parameters to be normalized arbitrarily. Here, the parameters have been normalized such that the parameters for neighboring Pt atoms are zero, and the parameter for no *CO neighbors is zero.

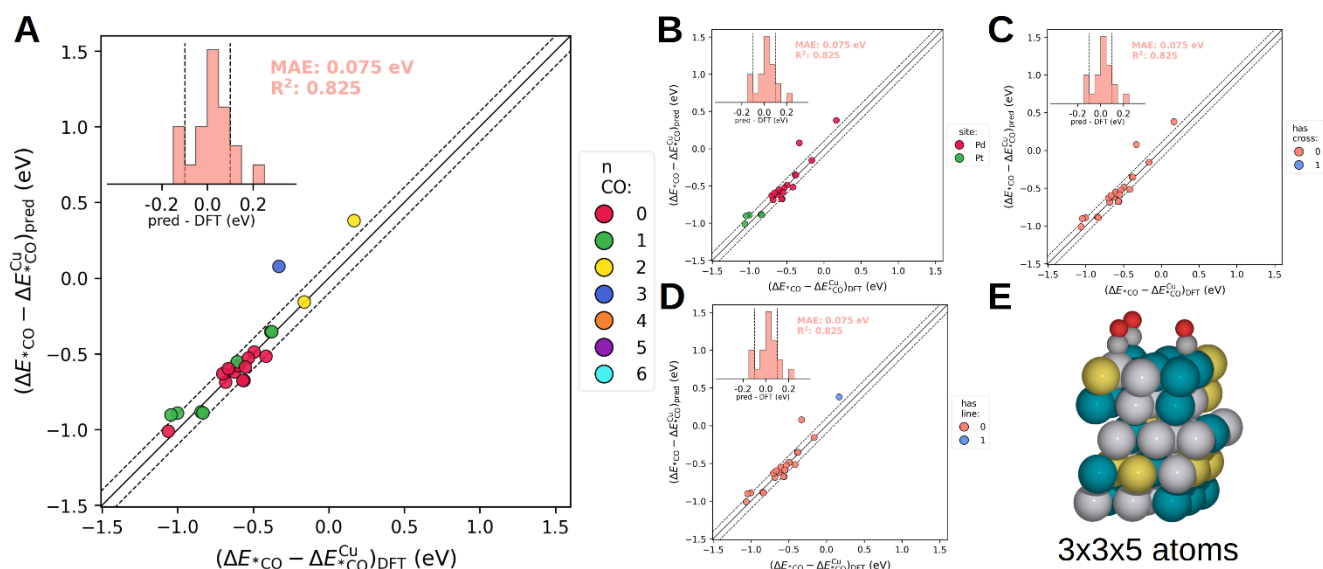| Feature	Specification	Parameter (eV)
Adsorption site	Pd	-0.470
	Pt	-0.943
Zone 1A	Ag	-0.069
	Au	-0.016
	Pd	-0.045
	Pt	0.000
Zone 2A	Ag	0.150
	Au	0.057
	Pd	0.029
	Pt	0.000
Zone 3B	Ag	-0.012
	Au	-0.040
	Pd	-0.011
	Pt	0.000
Number of *CO neighbors	0	0.000
	1	0.162
	2	0.311
	3	0.608
	4	0.910
	5	1.432
	6	1.890
Has line (0 or 1)		0.556
Has cross (0 or 1)		-0.802

Figure S9. Performance of *CO adsorption energy predictions on a 3x3x5 atom test set. **A-D**) Parity plots showing the performance (mean absolute error: 0.075 eV, coefficient of determination, R^2: 0.825) of the linear regression model obtained from the 3x2x5 atom surfaces of Figure S8 and Table S2 on a test set of 22 *CO adsorption energies on periodic 3x3x5 atom surfaces. The parity plots have been colored according to number of *CO neighbors (A), adsorption site (B), whether an 'X' is formed by the adsorbates (C), and whether a straight line is formed by the adsorbates (D). **E**) Example of a periodically repeated 3x3x5 atom structure used for generating the test set energies.
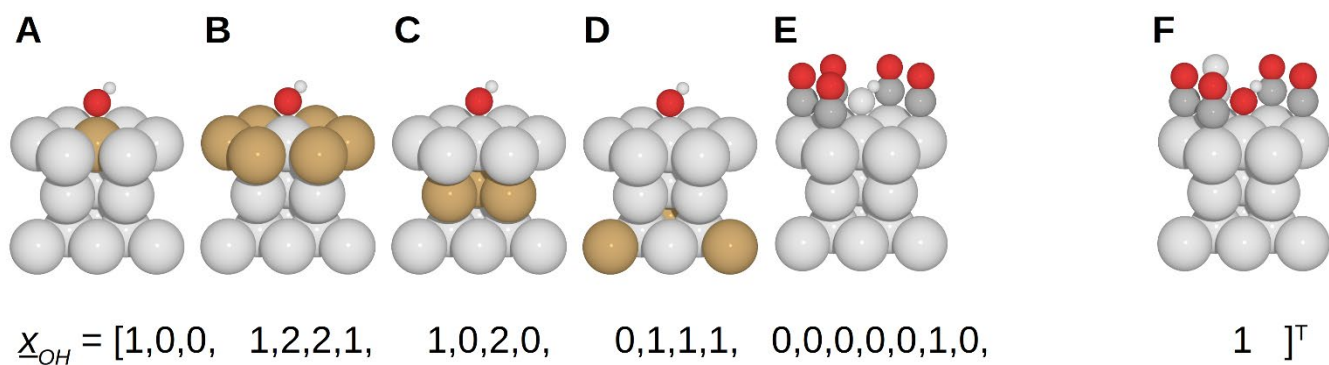
$\underline{x}_{OH}$ = [1,0,0,   1,2,2,1,   1,0,2,0,   0,1,1,1,   0,0,0,0,0,1,0,   1   ]^T

Figure S10. Feature construction and performance for *OH adsorption energy predictions. **A-F**) The feature vector consists of 23 numbers: 3 for identifying the on-top adsorption site (Ag, Pd, or Pt) (A); 4 obtained by counting the number of each element (in the order Ag, Au, Pd, and Pt) in the neighboring surface environment around the adsorbate (B); 4 by counting the elements in the neighboring subsurface (C); 4 by counting the elements in the next nearest zone of element in the 3rd layer (D); 7 for characterizing the number of *CO neighbors, a one-hot encoding of a number between 0 and 6 (E); and 1 for identifying whether 5 adsorbates form an 'X' cross-shape (F). An example of a feature vector is given.
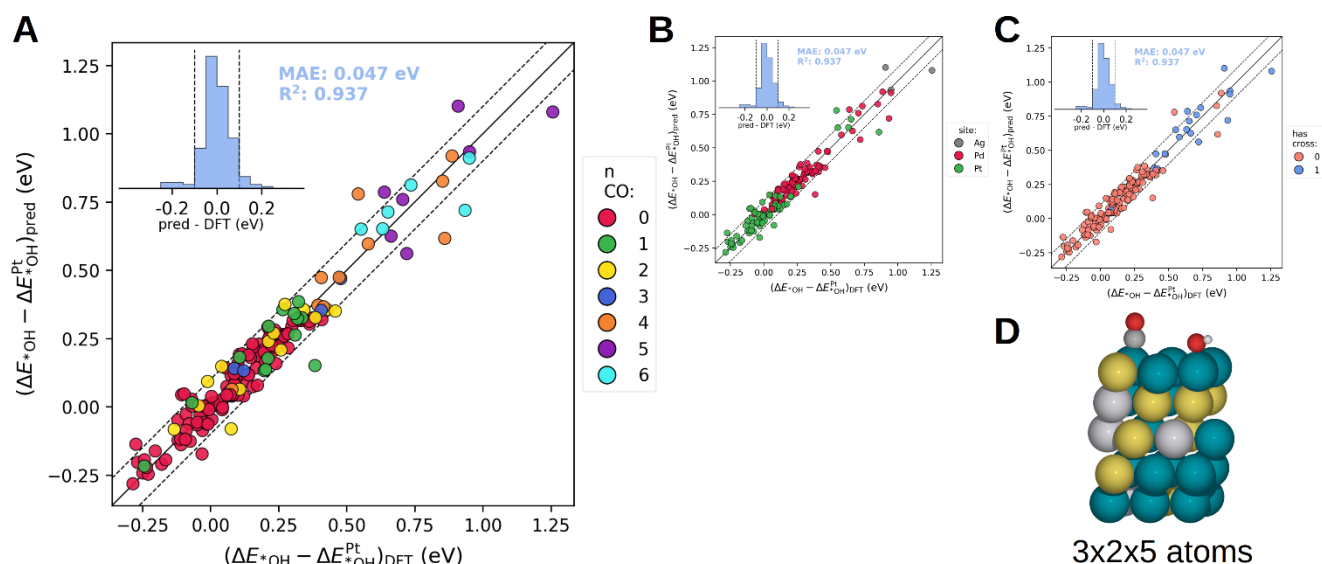
Figure S11. Performance of *OH adsorption energy predictions on a 3x2x5 atom training set. **A-C**) Parity plots showing the performance (mean absolute error: 0.047 eV, coefficient of determination, R^2: 0.937) of leave-one-out cross validations on linear regressors using 179 *OH adsorption energies obtained on periodic 3x2x5 atom surfaces. The parity plots have been colored according to number of *CO neighbors (A), adsorption site (B), and whether an 'X' is formed by the adsorbates (C). **D**) Example of a periodically repeated 3x2x5 atom structure used for generating the input energies.

Table S3. Linear parameters used for predicting *OH adsorption energies relative to *OH on Pt(111). The parameters correspond to the feature vector illustrated in Figure S10. The set of features contain 5 redundant variables due to the fixed number of atoms in the zones around the adsorbate. This allows the parameters to be normalized arbitrarily. Here, the parameters have been normalized such that the parameters for neighboring Pt atoms are zero, and the parameter for no *CO neighbors is zero.

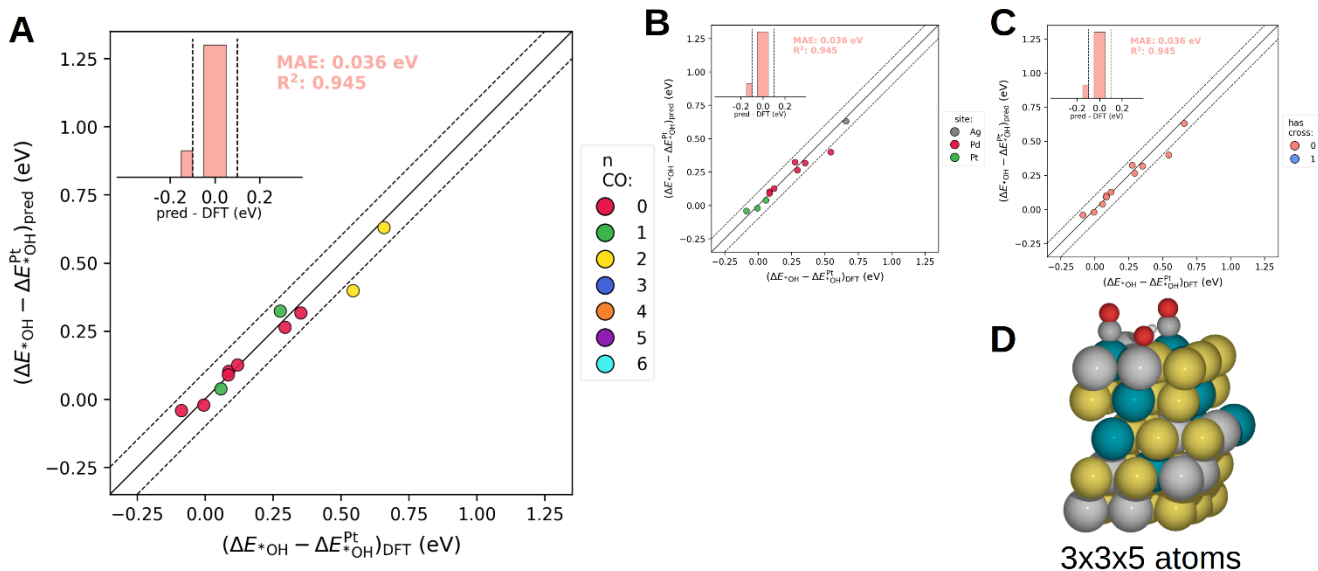| Feature	Specification	Parameter (eV)
Adsorption site	Ag	0.600
	Pd	0.248
	Pt	-0.023
Zone 1A	Ag	-0.071
	Au	-0.004
	Pd	-0.043
	Pt	0.000
Zone 2A	Ag	0.078
	Au	0.049
	Pd	0.031
	Pt	0.000
Zone 3B	Ag	0.020
	Au	-0.018
	Pd	-0.010
	Pt	0.000
Number of *CO neighbors	0	0.000
	1	0.060
	2	0.134
	3	0.247
	4	0.720
	5	0.960
	6	1.138
Has cross (0 or 1)		-0.445

Figure S12. Performance of *OH adsorption energy predictions on a 3x3x5 atom test set. **A-C**) Parity plots showing the performance (mean absolute error: 0.036 eV, coefficient of determination, R^2: 0.945) of the linear regression model obtained from the 3x2x5 atom surfaces of Figure S11 and Table S3 on a test set of 11 *OH adsorption energies on periodic 3x3x5 atom surfaces. The parity plots have been colored according to number of *CO neighbors (A), adsorption site (B), and whether an 'X' is formed by the adsorbates (C). **D**) Example of a periodically repeated 3x3x5 atom structure used for generating the test set energies.

Table S4. Onset dissolution/oxidation potentials and simulated surface energy of the metals used in the HEA in acidic media.

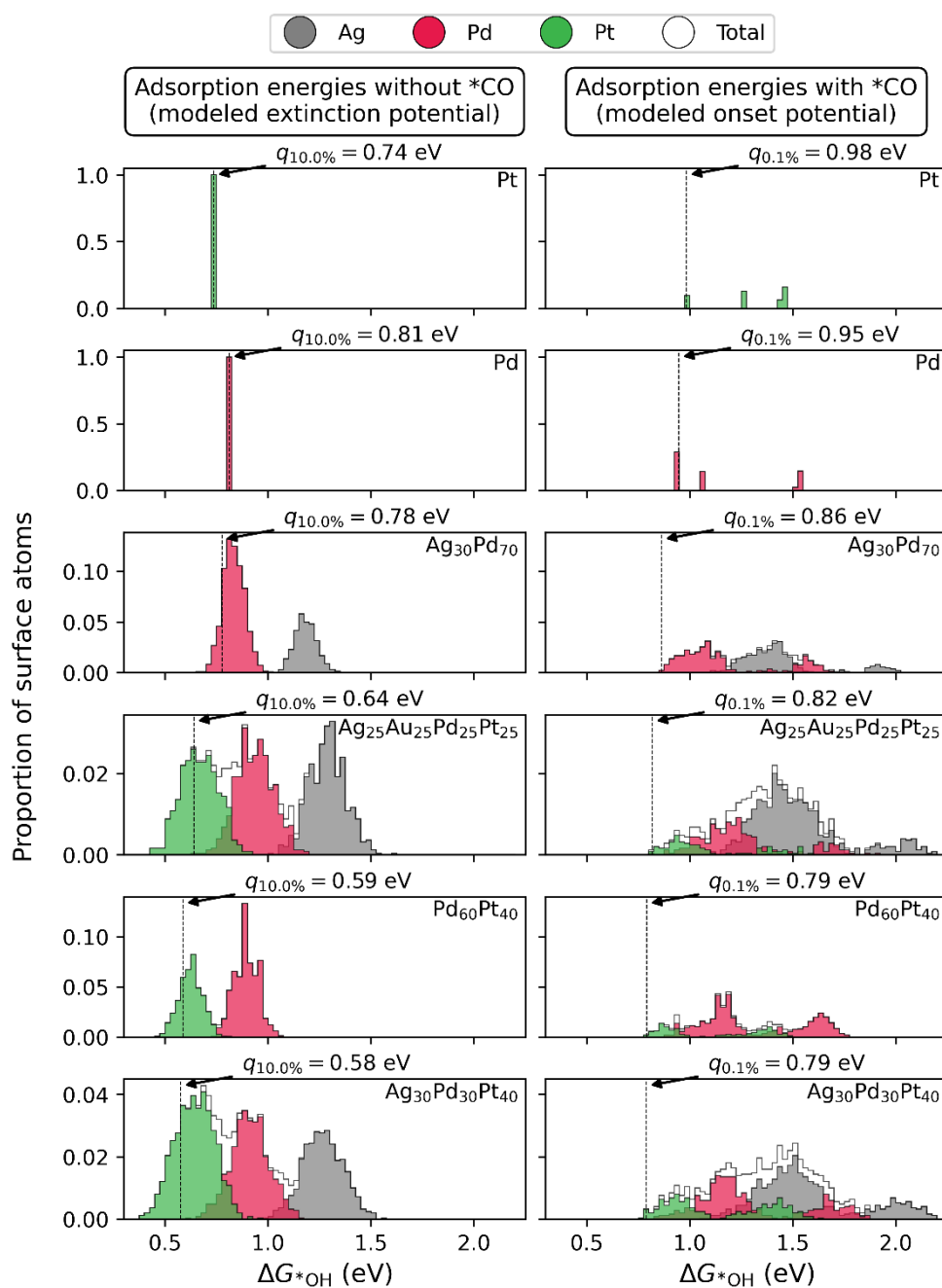| Metals	Potential V vs RHE	Simulated surface energy of (111) facet (eV / Å²) [5]
Cu	0.34 [3]	0.084
Ag	0.79 [3]	0.048
Pd	0.86 [3]	0.085
Pt	1.05-1.1 [4]	0.093
Au	1.40 [4]	0.044

Figure S13. Modeled *OH adsorption energy distributions for six selected compositions. The left column shows *OH adsorption energies on a surface without preadsorbed CO, the right column shows the corresponding surface with preadsorbed CO. The percentiles of strongest *OH adsorption energies used to obtain the onset and extinction potentials for Figure 6 in the main text are shown with dashed vertical lines.

References

(1)   Rumble, J. R.; Bickham, D. M.; Powell, C. J. The NIST X-ray Photoelectron Spectroscopy Database. *Surface and Interface Analysis* **1992**, *19* (1–12), 241–246. https://doi.org/10.1002/sia.740190147.

(2)   Moulder, F. J.; Stickle, F. W.; Sobol, E. P.; Bomben, D. K. *Handbook of X-Ray Photoelectron Spectroscopy (XPS)*; 2005. https://doi.org/10.1002/0470014229.ch22.

(3)   Pourbaix, M. *Atlas of Electrochemical Equilibria in Aqueous Solutions*; 1974; Vol. 2. https://doi.org/10.1016/0022-0728(67)80059-7.

(4)   Cherevko, S.; Zeradjanin, A. R.; Keeley, G. P.; Mayrhofer, K. J. J. A Comparative Study on Gold and Platinum Dissolution in Acidic and Alkaline Media. *Journal of The Electrochemical Society* **2014**, *161* (12), H822–H830. https://doi.org/10.1149/2.0881412jes.

(5)   Tran , R.; Xu, Z.; Radhakrishnan, B.; Winston, D.; Sun, W.; Persson, K. A.; Ong, S. P. Surface Energies of Elemental Crystals. *Scientific Data* **2016**, 3, 160080. https://doi.org/10.1038/sdata.2016.80. Data made graphically available at http://crystalium.materialsvirtuallab.org.